JOURNAL OF ENDOUROLOGY
Volume 29, Number 7, July 2015

Pp. 810–815
DOI: 10.1089/end.2014.0585

Histotripsy of the Prostate in a Canine Model: Characterization of Post-Therapy Inflammation and Fibrosis

Sarah E. Darnell, MSE,[1] Timothy L. Hall, PhD,[1] Scott A. Tomlins, MD, PhD,[2] Xu Cheng, MD,[3] Kimberly A. Ives, DVM,[1] and William W. Roberts, MD[3]

Abstract

Introduction: Histotripsy is a nonthermal, noninvasive, pulsed ultrasound technology that homogenizes tissue within the targeted volume. From previous experiments, it appeared that the resultant fibrotic response from histotripsy was limited compared with the typical tissue response seen after thermoablation. The objective of this study was to characterize the inflammatory response and quantify patterns of collagen deposition 6 weeks after *in vivo* canine prostate histotripsy.

Methods: Histotripsy was applied to the left half of eight canine prostates to produce an intraparenchymal zone of tissue homogenization. Six weeks after treatment, prostates were harvested, sectioned, and stained with hematoxylin and eosin for histologic evaluation, CD3, CD20, and Mac387 immunohistochemistry to characterize the inflammatory components, and picrosirius red staining to identify collagen.

Results: Seven of eight treated prostates exhibited only minimal residual inflammation. Visual microscopic analysis of picrosirius red slides revealed a band of dense collagen (0.5 mm wide) immediately adjacent to the cavity produced by histotripsy. This was surrounded by a second band (1 mm wide) of less dense collagen interspersed among glandular architecture. A lobar distribution of epithelial atrophy and basal cell hyperplasia reminiscent of periurethral glands and ducts was apparent surrounding the margin of the treatment cavities. Tissue loss (-31%) was apparent on the treated side of all prostates while four demonstrated a net decrease in collagen content.

Conclusions: *In vivo* histotripsy of canine prostate produced a decrease in prostate volume coupled with a limited inflammatory and fibrotic response. A narrow (1.5 mm) band of fibrosis around the empty, re-epithelialized treatment cavity was observed 6 weeks after treatment. In four cases, an overall reduction in collagen content was measured. Further studies are planned to correlate these histologic findings with alteration in mechanical tissue properties and to explore histotripsy strategies for treatment of benign prostatic hyperplasia that optimize tissue volume removal with minimization of fibrosis.

Introduction

Fibrosis within the prostate has recently been implicated as a contributing factor in the etiology of lower urinary tract symptoms (LUTS) from benign prostatic hyperplasia (BPH).[1,2] Conventional teaching holds that mechanical obstruction from enlarging prostatic adenoma (static factor) and increased smooth muscle tone (dynamic factor) are the source of LUTS. It is believed, however, that excessive myofibroblast activity within the prostate and increased collagen deposition increases tissue stiffness and thereby decreases urethral function.[1] Fibrosis has also been linked to organ dysfunction and disease of the pancreas, lungs, liver, kidney, and bowel.[3–5]

Recent pilot studies analyzing prostatic tissue support an association between collagen content/prostatic fibrosis and LUTS in specimens obtained from radical prostatectomy.[1,2] Additional research in a mouse model has bolstered the evidence supporting a causative relationship between fibrosis and LUTS.[6] It therefore seems plausible that treatment modalities that debulk overgrown adenomatous tissue and/or reduce fibrosis, may provide the best opportunity for LUTS improvement.

Histotripsy is a noninvasive ablative acoustic technology that destroys targeted tissue by inducing acoustic cavitation (microbubble formation) to mechanically homogenize cellular and connective (collagen) components of tissue, without producing thermal coagulative necrosis. As a result, histotripsy

Departments of [1]Biomedical Engineering, [2]Pathology, and [3]Urology, University of Michigan, Ann Arbor, Michigan.

can be tightly confined with only a narrow marginal zone of sublethal damage. The feasibility of histotripsy tissue homogenization (producing a transurethral resection of the prostate [TURP]-like defect) has been previously demonstrated in canine models.[7–9] Typically, the margin of the treatment cavity exhibited only a limited fibrotic response and was repopulated with urothelium within 3 to 4 weeks of histotripsy.[10,11]

The current study was conducted to explore the fibrotic response after histotripsy. Specifically, we sought to characterize the inflammatory response and quantify patterns of collagen deposition 6 weeks after *in vivo* canine prostate histotripsy.

Methods

Eight intact male mongrel dogs were used for this study with the approval of the Institutional Animal Care and Use Committee. The canine subjects were prepared for histotripsy as reported previously.[12] Briefly, after administration of antibiotic prophylaxis and analgesia, canines were anesthetized, intubated, and maintained under inhalational anesthesia. The suprapubic region was shaved and a soap suds enema performed to evacuate the rectum before positioning supine on the procedural table. Transrectal ultrasonography (TRUS) using a Logiq P6 US scanner and ERB probe (GE Healthcare, Waukesha, WI) in a custom holder facilitated targeting and provided image feedback during treatment.

The histotripsy transducer, an 11×14 cm oval-shaped piezoceramic composite array (750 kHz frequency, 10 cm focal length; Imasonic, Inc., Voray-sur-l'Ognon, FR), generated an approximate $3 \times 3 \times 8$ mm bubble cloud. This device was suspended from a three-axis computer-controlled positioning system (MATLAB, MathWorks, Natick, MA) above the abdomen with acoustic coupling achieved by placing the histotripsy transducer in a bolus of degassed water contained within a thin plastic membrane on the shaved abdomen (Fig. 1).

Each dog underwent histotripsy treatment by sequential targeting of a grid of distinct points (spaced by 6–9 mm) within the left hemiprostate to avoid the urethra. The number of distinct target points varied (5–11), depending on the prostate size and shape. Each target point was treated for 120 seconds at a pulse repetition frequency of 500 Hz (60,000 pulses). After treatment, canine subjects were monitored with daily veterinary evaluations assessing hematuria, urinary retention, pain, and changes in dietary pattern or behavior. Flexible cystourethroscopy (8.2F Dur-8 flexible ureteroscope) was performed to inspect the bladder and prostatic urethra immediately post-treatment and weekly thereafter. TRUS imaging was performed to assess for treatment effect weekly.

Six weeks after treatment, the canine subjects were sacrificed, and the prostates harvested. Two prostates obtained from untreated subjects in an unrelated study were used as controls. Specimens were fixed in formalin for 1 week, cut into 5 mm thick slices, dehydrated with 24% ethanol, and embedded in paraffin. Transverse sections (5 μm thick) were cut at 1 mm increments through the prostate, mounted, and stained with hematoxylin and eosin for histologic evaluation. CD3, CD20, and Mac387 immunohistochemistry were performed to characterize the inflammatory components, and picrosirius red staining was performed to identify collagen. Each half-prostate (divided by a vertical midline through the urethra) was examined and inflammation quantified on a 0-4 scale: 0–no inflammation, 1–rare interstitial inflammation, 2–rare inflammatory foci (including follicle formation), 3–frequent inflammatory foci, and 4–diffuse confluent inflammation. Histopathologic evaluation was performed by a board certified anatomic pathologist with subspecialty expertise in genitourinary pathology (SAT).

Imaging methods, similar to those reported by Juodziukyniene and associates,[13] were used to quantify collagen. Microscopic images of picrosirus red stained slides were captured at 20x magnification (pixel size 3.7 μm), and images of whole transverse prostate images at 2400 dots per inch (dpi) resolution (pixel size 10.6 μm) were acquired with a flatbed scanner. Red pixels were categorized as containing collagen. ''Collagen content'' was defined as the area occupied by red pixels and ''collagen density'' as the percentage of red pixels within each defined region of interest.

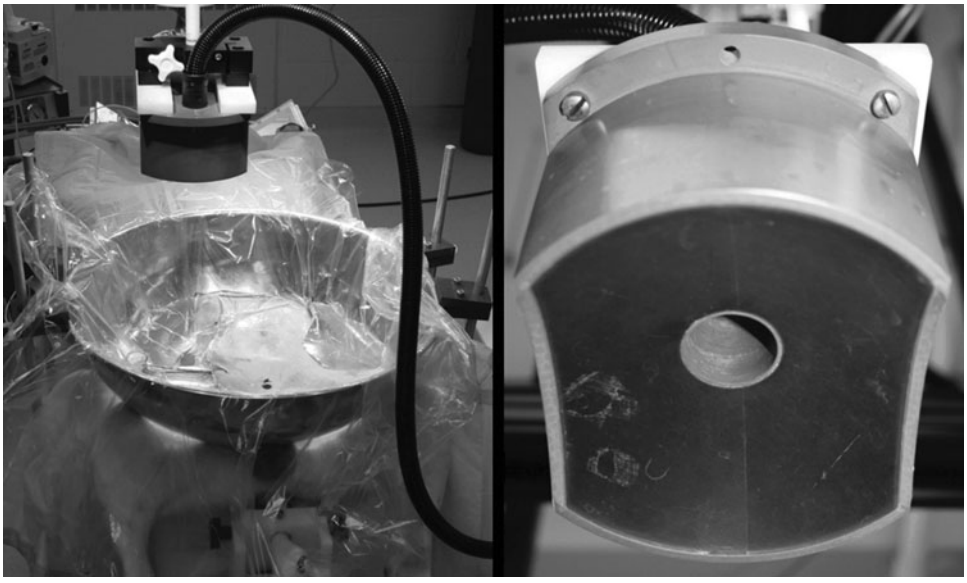

FIG. 1. Apparatus for canine prostate histotripsy treatment. An anesthetized canine is positioned supine with transrectal ultrasonography probe inserted in the rectum. The histotripsy therapy transducer suspended over the shaved abdomen is positioned within the degassed water bath for acoustic coupling when delivering energy to the prostate.

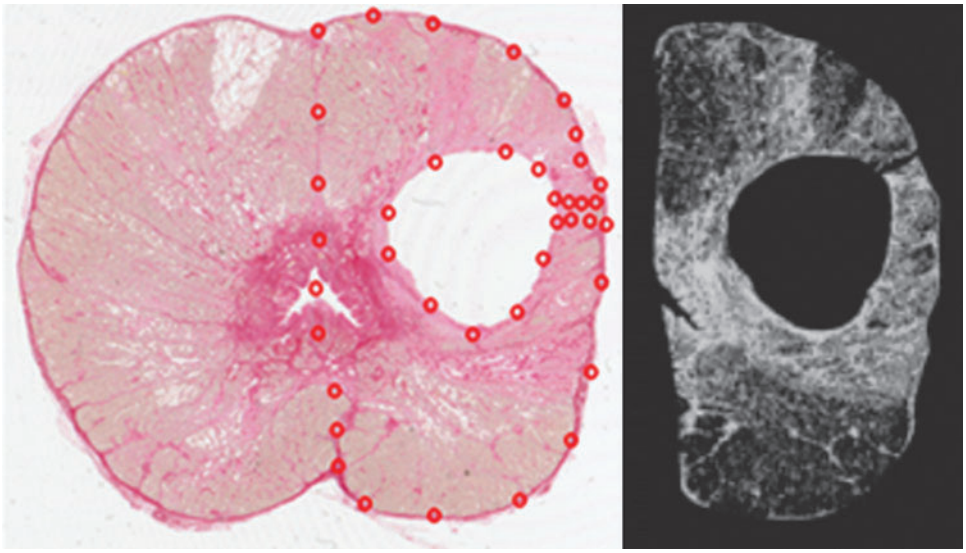

FIG. 2. A 2400 dots per inch scan of a prostate section from subject 2 stained with picrosirius red (*left*) for collagen identification. The histotripsy treatment cavity is evident in the left hemiprostate. The red dots define the region of interest used to calculate the tissue collagen density and tissue area. The empty treatment lesion was excluded from the region of interest. A binary, black and white rendering (*right*) of the treated hemiprostate is shown with collagen containing pixels displayed as white.

The 20x magnified images were captured at eight locations along the perimeter of the treatment cavities (the 3, 6, 9, and 12 o'clock locations and the associated intermediate locations) to assess the margin of the treatment cavity and immediate adjacent tissue. The images taken from the flatbed scanner encompassed the entire transverse section of the prostate and were used to macroscopically compare the treated and control (untreated) halves of each prostate that were segmented by tracing the vertical anatomic midline through the center of the urethra. Treatment cavities, devoid of tissue, were excluded from the image analysis (Fig. 2).

Results

In vivo canine histotripsy produced a cavitation bubble cloud, visualized within the prostate and monitored with TRUS imaging, in all cases. There were no treatment-related complications during or after treatment. Weekly TRUS assessment revealed development of anechoic cavities within the targeted prostate volumes in each left hemiprostate.

On histologic examination, the treatment side of each prostate exhibited a vacuous cavity that corresponded to the histotripsy treatment volume. These cavities were epithelialized and demonstrated urothelium with squamous metaplasia. A narrow band of loose fibromuscular stroma (1.5 mm width [range: 0.5–2.6 mm]) was present surrounding each treatment cavity (Fig. 3). On high power, the fibromuscular stroma band was composed of two concentric fibrotic bands. The average collagen density was found to be 85% in the inner band and 75% in the outer band (Table 1).

The surrounding prostate glands showed lobular areas of epithelial atrophy and basal cell hyperplasia interspersed with unremarkable prostate glands, which varied across cases. These areas of atrophy/basal cell hyperplasia were reminiscent of periurethral glands and ducts (Fig. 4). No specific relationship between histotripsy treatment and inflammation was apparent. Areas of atrophy/basal cell hyperplasia adjacent to histotripsy cavities had mildly increased interstitial chronic inflammation, as is appreciable in basal cell hyperplasia in other contexts.

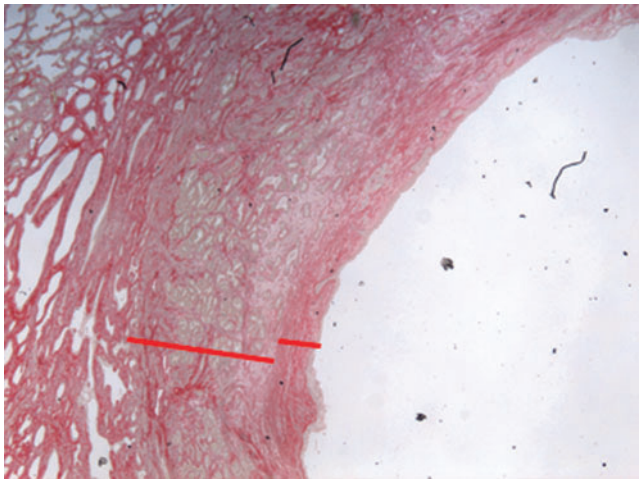

FIG. 3. Representative portion of a 20× magnified image displaying the histotripsy treatment cavity as well as extent of the surrounding inner and outer fibrotic bands, designated on the image.

Table 1. Characterization of Collagen Deposition/Fibrosis Surrounding Histotripsy Treatment Cavities

	Collagen band width			*Collagen density*	
Subject	*Inner (mm)*	*Outer (mm)*	*Total (mm)*	*Inner*	*Outer*
1	0.3	0.4	0.7	84%	50%
2	0.3	0.9	1.3	91%	81%
3	0.6	1.3	1.9	87%	84%
4	0.5	1.6	2.2	73%	66%
5	0.5	1.3	1.8	96%	88%
6	0.3	0.6	0.9	92%	89%
7	0.1	0.4	0.5	97%	90%
8	1.3	1.4	2.6	59%	56%
Average	0.5	1.0	1.5	85%	75%

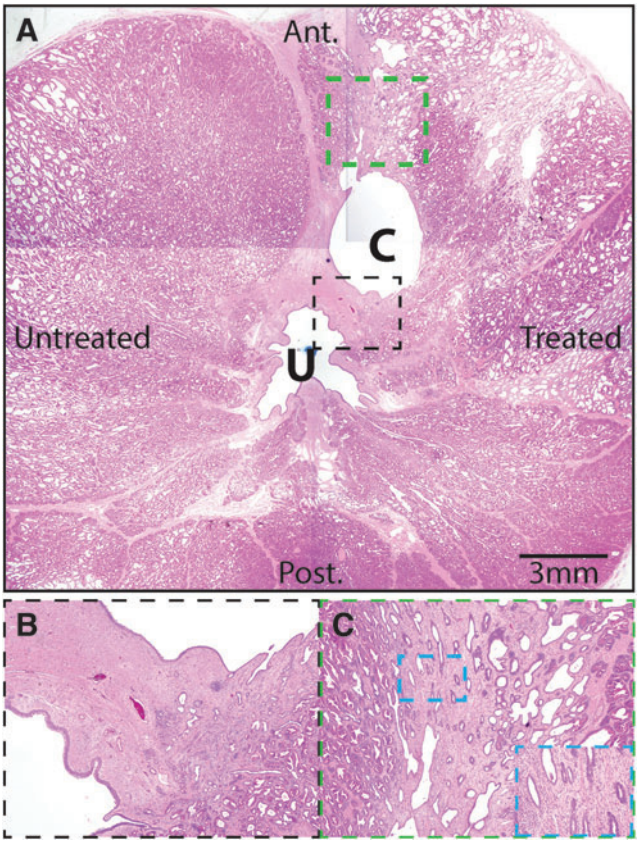

FIG. 4. Representative histopathology of histotripsy-treated canine prostate. (**A**) A composite image of a histotripsy-treated canine prostate (subject 7). Anterior (Ant.) and posterior (Post.) are indicated, along with the treated and untreated sides. The urethra (U) and cavitation cavity (C) are noted. Minimal interstitial inflammation was noted in the treated and untreated sides in this subject. Indicated areas shown in dashed black and green boxes are shown as insets in B and C. (**B**) The reepithelialized cavitation cavity is surrounded by fibromuscular stroma similar in appearance to that surrounding the urethra. (**C**) Foci of atrophic glands and basal cell hyperplasia surround the cavitation cavity, reminiscent of periurethral ducts/glands. In addition, areas of unremarkable prostate glands were also adjacent to the cavitation cavity. Higher power view of atrophy and basal cell hyperplasia with surrounding minimal interstitial chronic inflammation is shown in the inset. Original magnifications 1.25× (A), 4× (B), 10× (C), and 20× (inset of C).

The contralateral untreated side of each prostate demonstrated no appreciable effect from histotripsy and appeared similar to control prostate specimens. The control prostates and both treated and untreated sides of the experimental prostates showed predominantly mild interstitial chronic inflammation (B-cells, T-cells, and plasma cells) with rare lymphoid follicles. In a single case (subject 8), the histotripsy cavity, which communicated with the urethra, had features of a prostatic abscess, including intraepithelial acute inflammation, epithelial ulceration, markedly increased macrophages, acute and chronic (B-cell, T-cell, and plasma cells) inflammation.

Tissue loss was visually apparent on the treated side of each prostate (Fig. 5). Comparison of cross-sectional areas of

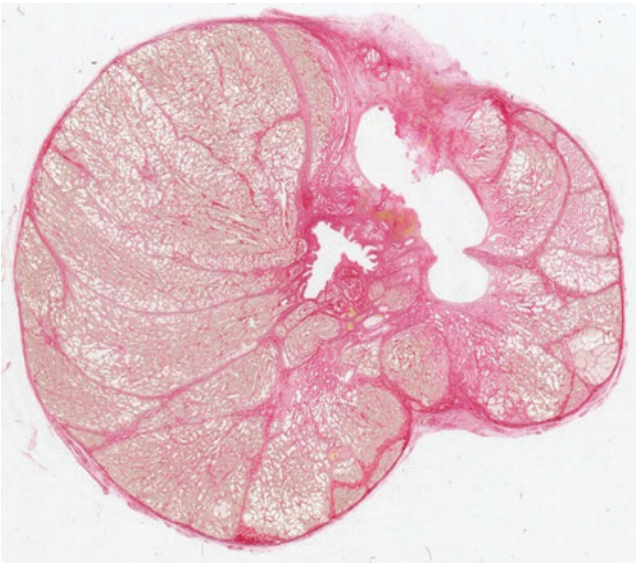

FIG. 5. This 2400 dots per inch scan of a picrosirius red stained prostate section demonstrates a partially collapsed histotripsy treatment cavity and tissue volume loss on the left side of the prostate compared with the untreated right side of the prostate. The measured cross-sectional tissue area of the left hemiprostate was 2.4 cm^2 less than the right.

the treated and untreated halves of each prostate revealed an average of 1.5 cm^2 (range 0.3–3.1 cm^2) less prostate tissue on each treated half. Assuming pretreatment symmetry of each prostate, this represents a mean 31% loss of tissue area (Table 2). Four of the histotripsy-treated prostate halves demonstrated a net increase in collagen content, while four demonstrated a net decrease in collagen content (range −21% to +33%).

Although histotripsy treatment was delivered to the prostate with the intent of ''sparing'' the urethra (i.e., producing zones of homogenate that would be resorbed rather than drain via the urethra), in three cases (subjects 3, 7, 8) the treatment cavity was seen to communicate with the urethra (Fig. 6). In subject 7, the treatment cavity was within 1 mm of the urethral lumen with disruption of periurethral tissue and was considered to have been in communication in an adjacent tissue plane. In the other five cases, the periurethral smooth muscle and connective tissue appeared intact with at least 2 mm tissue thickness between the treatment cavity and urethral lumen (Figs. 2, 5).

Discussion

Histotripsy destroys tissue by mechanical means and produces tissue liquefaction. In this study, seven of eight subjects exhibited only minimal residual inflammation 6 weeks after treatment equivalent to baseline. Tissue destruction was apparent by an empty reepithelialized treatment cavity surrounded by a thin band of fibrosis. On the treated half of each prostate, a pattern of epithelial atrophy and basal cell hyperplasia was noted, which appeared reminiscent of conventional periurethral glands/ducts. In contrast, thermoablative modalities (transurethral needle ablation [TUNA], microwave therapy, high intensity focused ultrasound [HIFU], interstitial laser, etc.) are designed to heat tissue to cause immediate cell death and protein coagulation (histology coagulation

Table 2. Comparison of the Treated and Untreated Half of Each Prostate and Control Data

	Treated half				*Untreated half*					
Subject	*Area (cm^2)*	*Inflam. score*	*Collagen content (cm^2)*	*Collagen density (%)*	*Area (cm^2)*	*Inflam. score*	*Collagen content (cm^2)*	*Collagen density (%)*	*Change in area (cm^2)*	*Change in collagen content (cm^2)*
1	3.4	1	1.0	31	4.8	1	0.9	19	−1.4 [−29%]	0.1 [11%]
2	3.0	2	1.2	38	3.8	2	0.9	24	−0.8 [−21%]	0.3 [33%]
3	2.5	2	1.1	43	3.7	2	1.4	38	−1.2 [−32%]	−0.3 [−21%]
4	3.0	1	1.2	42	6.1	2	1.1	18	−3.1 [−51%]	0.1 [9%]
5	4.6	2	2.0	42	7.0	3	2.1	30	−2.4 [−34%]	−0.1 [−5%]
6	5.8	3	1.8	32	7.6	3	1.7	22	−1.8 [−24%]	0.1 [6%]
7	2.5	0	1.9	79	2.8	1	2.1	73	−0.3 [−11%]	−0.2 [−10%]
8	1.8	2	1.4	75	2.8	4	1.7	62	−1.0 [−36%]	−0.3 [−18%]
Mean	3.3	1.6	1.4	48	4.8	2.2	1.5	36	−1.5 [−31%]	−0.1 [−7%]
C1 right					4.4	3	2.1	49		
C1 left					4.6	3	2.5	55		
C2 right					4.9	2	1.8	36		
C2 left					4.9	2	1.9	40		

necrosis).[14] This generates an inflammatory response that commonly leads to dense fibrosis and scarring.[15]

In a comprehensive review of microwave, TUNA, HIFU, and interstitial laser ablation treatment for BPH, Larson and colleagues[16] describe histologic findings of devitalized tissue with a border of fibrosis and granulation tissue. In a study of 10 men with BPH who underwent TUNA, dense fibrosis or scarring with adjacent areas of squamous metaplasia was found in the three men who needed subsequent TURP.[17]

FIG. 6. 2400 dots per inch image of a picrosirius red stained prostate section from subject 3. The histotripsy treatment cavity is seen to communicate with the urethral lumen with collagen deposition apparent surrounding the treatment zone.

Fibrosis was also seen in several studies of thermal ablation of prostate tissue in canine models. One study of radiofrequency ablation demonstrated dense char within the prostate treatment areas immediately after treatment—histologically consistent with coagulative necrosis.[18] Similarly, histologic analysis of canine prostates harvested 0 to 12 weeks after HIFU treatment revealed discolored lesions of tissue coagulative necrosis and hemorrhage, with an inflammatory response, eventually forming a cystic cavity or region of fibrosis and scarring.[19]

In this study, the overall extent of collagen deposition and fibrosis after histotripsy appeared to be less than what has been described for thermoablative modalities. The net change in collagen content after histotripsy is likely the summation of several competing factors. Some collagen is destroyed with tissue homogenization, evidenced by a vacuous treatment cavity. There appears to be collagen deposition surrounding the treatment cavity, although only in a narrow band (1.5 mm). Beyond this zone there was marked tissue volume loss (-31%) with apparent consolidation of preexisting collagen and preferential shrinkage of the usual glandular epithelial component. In four cases there appeared to be net loss of collagen and in four cases a net increase of collagen within the treated half of each prostate.

These results suggest that in certain cases, it may be possible to decrease collagen content within the prostate, which can be hypothesized to lead to decreased tissue stiffness and improved urethral compliance. Further work to test this hypothesis is planned and will include tissue measures of stiffness (Young's modulus) both physically at prostate harvest and nondestructively with new methods of prostate tissue ultrasound elastography. In addition, the clinical significance of changing the mechanical properties of the prostate needs to be assessed with clinically meaningful urodynamic measures and ultimately assessment of LUTS.

This initial pilot study was limited by several factors including small sample size. Ideally, a model system less subject to prostate tissue heterogeneity is needed. Even untreated control prostate specimens exhibited marked heterogeneity of collagen density and inflammation, which is consistent with the known histologic variability of BPH. To overcome this limitation, only the left half of each prostate

was treated, allowing the right half to serve as an internal control in each case.

The image quantification algorithm is subject to an overestimation area when calculating the absolute collagen area. Because collagen fiber widths can be as small as several nanometers, even the presence of a very small amount of stained collagen within a pixel will result in it being characterized as a collagen containing pixel. This overestimation of collagen area will be greatest when assessing low magnification images, which have the largest pixel size. As image magnification increases, pixel size decreases, and the effect of overestimation decreases. Nonetheless, when comparing images of the same magnification, this image analysis algorithm does allow relative comparison of collagen content.

Conclusions

In vivo histotripsy of canine prostate produced a decrease in prostate volume coupled with a limited inflammatory and fibrotic response. A narrow (1.5 mm) band of fibrosis around the empty, reepithelialized treatment cavity was observed 6 weeks after treatment. In four cases, an overall reduction in collagen content was measured after histotripsy. Further studies are planned to correlate these histologic findings with alteration in mechanical tissue properties and to explore histotripsy strategies for treatment of BPH that optimize tissue volume removal with minimization of fibrosis.

Acknowledgments

Funding: R01 DK087871; SAT is supported by the A. Alfred Taubman Medical Research Institute.

Author Disclosure Statement

Timothy L. Hall and William W. Roberts have royalty, equity, and consulting interests with HistoSonics, Inc.. For the remaining authors, no competing financial interests exist.

References

1. Ma J, Gharaee-Kerman M, Kunju L, et al. Prostate fibrosis is associated with lower urinary tract symptoms. J Urol 2012;188:1375–1381.
2. Cantiello F, Cicione A, Salonia A, et al. Periurethral fibrosis secondary to prostatic inflammation causing lower urinary tract symptoms: A prospective cohort study. Urology 2013;81:1018–1023.
3. Apte M, Pirola R, Wilson J. The fibrosis of chronic pancreatitis: New insights into the role of pancreatic stellate cells. Antioxid Redox Signal 2011;15:2711–2722.
4. Datta A, Scotton CJ, Chambers RC. Novel therapeutic approaches for pulmonary fibrosis. Br J Pharmacol 2011;163: 141–172.
5. Novo E, di Bonzo LV, Cannito S, et al. Hepatic myofibroblasts: A heterogeneous population of multifunctional cells in liver fibrogenesis. Int J Biochem Cell Biol 2009;41:2089–2093.
6. Gharaee-Kermani M, Rodriguez-Nieves JA, Mehra R, et al. Obesity-induced diabetes and lower urinary tract fibrosis promote urinary voiding dysfunction in a mouse model. Prostate 2013;73:1123–1133.
7. Xu Z, Raghaven M, Hall TL, et al. High speed imaging of bubble clouds generated in pulsed ultrasound cavitational therapy—histotripsy. IEEE Trans Ultrason Ferroelectr Freq Control 2007;54:2091–2101.
8. Kieran K, Hall TL, Parsons JE, et al. Refining histotripsy: Defining the parameter space for the creation of nonthermal lesions with high intensity, pulsed ultrasound of the in vitro kidney. J Urol 2007;178:672–676.
9. Winterroth F, Xu Z, Wang TY, et al. Examining and analyzing subcellular morphology of renal tissue treated by histotripsy. Ultrasound Med Biol 2011;37:78–86.
10. Hempel CR, Hall TL, Cain CA, et al. Histotripsy fractionation of prostate tissue: Local effects and systemic response in a canine model. J Urol 2011;185:1484–1489.
11. Roberts WW, Teofilovic D, Jahnke RC, et al. Histotripsy of the prostate using a commercial system in a canine model. J Urol 2014;191:860–865.
12. Schade GR, Styn NR, Ives KA, et al. Prostate histotripsy: Evaluation of prostatic urethral treatment parameters in a canine model. BJU Int 2014;113:498–503.
13. Juodziukyniene N, Aniuliene A, Pangonyte D. Effect of age, hyperplasia, and atrophy on collagen parameters in dog prostates. Pol J Vet Sci 2010;13:479–485.
14. Goldberg SN, Gazelle GS, Mueller PR. Thermal ablation therapy for focal malignancy: A unified approach to underlying principles, techniques, and diagnostic imaging guidance. AJR Am J Roentgenol 2000;174:323–331.
15. Denisov-Nikol'skii YI, Shafranov VV, Mazokhin VN, et al. Morphologic changes in the liver after microwave destruction. Bull Exp Biol Med 2001;131:377–381.
16. Larson BT, Bostwick DG, Corica AG, Larson TR. Histological changes of minimally invasive procedures for the treatment of benign prostatic hyperplasia and prostate cancer: Clinical implications. J Urol 2003;170:12–19.
17. Harewood LM, Cleeve LK, O'Connell HE, et al. Transurethral needle ablation of the prostate (TUNA): Clinical results and ultrasound, endoscopic, and histologic findings in pilot study of patients in urinary retention. J Endourol 1995;9:407–412.
18. McGahan JP, Griffey SM, Budenz RW, Brock JM. Percutaneous ultrasound-guided radiofrequency electrocautery ablation of prostate tissue in dogs. Acad Radiol 1995;2:61–65.
19. Foster RS, Bihrle R, Sanghvi N, et al. Production of prostatic lesions in canines using transrectal administered high-intensity focused ultrasound. Eur Urol 1993;23:330–336.

Address correspondence to:
William W. Roberts, MD
Department of Urology
University of Michigan
3879 Taubman Center
Ann Arbor, MI 48109-5330

E-mail: willrobe@umich.edu

Abbreviations Used

BPH = benign prostatic hyperplasia
dpi = dots per inch
HIFU = high intensity focused ultrasound
LUTS = lower urinary tract symptoms
TRUS = transrectal ultrasonography
TUNA = transurethral needle ablation
TURP = transurethral resection of the prostate